POLITECNICO DI TORINO
Repository ISTITUZIONALE

Molecular Junctions for an Effective Readout in Molecular Field-Coupled Nanocomputing

(Article begins on next page)

11 May 2026

Molecular Junctions for an Effective Readout in Molecular Field-Coupled Nanocomputing

Federico Ravera*, Roberto Listo*‡, Fabrizio Mo*, Gabriele Farchetti*, Giuliana Beretta*,
Yuri Ardesi*, Gianluca Piccinini*, Mariagrazia Graziano†§

*Department of Electronics and Telecommunications, Politecnico di Torino, Torino, Italy
†Department of Applied Science and Technology, Politecnico di Torino, Torino, Italy
‡Department of Electrical, Computer and Biomedical Engineering, University of Pavia, Pavia 27100, Italy
§corresponding author e-mail: mariagrazia.graziano@polito.it

Abstract—The Molecular Field-Coupled Nanocomputing (MolFCN) is a candidate technology for future digital electronics devices. Unlike CMOS, MolFCN relies on a non-conductive principle, in which the binary information is encoded in the polarization state of molecules, enabling fast and low-power digital computation. Due to the different MolFCN and CMOS operating principles, the scientific community is still seeking solutions to enable the integration of MolFCN with CMOS electronics. In this work, we propose a method to transduce charge-based information encoding into electrical quantities using single-molecule junctions. In particular, we demonstrate, with *ab initio* calculation, that the OPE3 junction changes its conduction properties when exposed to a dipole moment. This work identifies molecular junctions as possible candidates for providing hybrid integration with CMOS, favoring the assessment of MolFCN technology.

I. INTRODUCTION

Molecular Field-Coupled Nanocomputing (MolFCN) is an ultra-low-power computational paradigm with promising applications in digital electronics. Based on the Quantum-dot Cellular Automata (QCA) model, it encodes binary information through charge distribution in electrostatically coupled molecules. MolFCN enables data propagation via electrostatic interactions [1], thus avoiding power dissipation due to currents at the information-transport scale [1], [2]. Fig. 1(a) shows the bis-ferrocene molecule used to encode information in MolFCN cells [3], [4]. MolFCN theoretically permits GHz-range processing while keeping functionality even at ambient temperature [5]–[8].

Despite the theoretical advantages, the fabrication of a functional MolFCN prototype remains challenging [9], [10]. The scientific community faces significant challenges, including the precise arrangement of molecular patterns, the clock fabrication for reliable data transport, and the integration of information readout with CMOS technology [9], [11]–[14]. Recent studies have explored promising readout methods using spectroscopy or single-electron transistors [15]–[17]. Still, the available approaches face limitations in device integration and room-temperature operation, which are considered fundamental advantages of MolFCN.

This work investigates the usage of Single-Molecule Junctions (SMJs) as amperometric sensors of the molecular electric dipole to enable MolFCN readout in an integrated
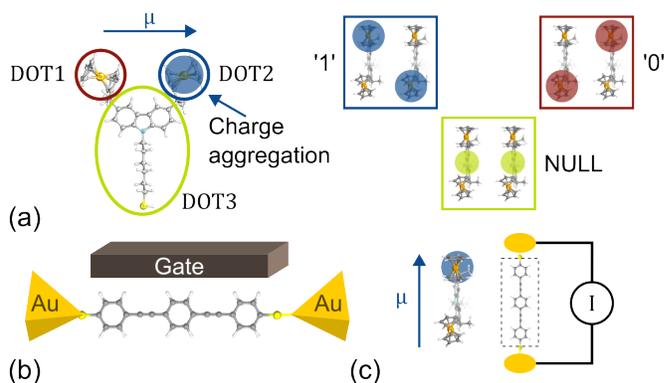

Fig. 1. (a) Bis-ferrocene cation used for encoding logic MolFCN information by aggregating charge into dots. The charge distribution creates a dipole moment. Two molecules can be used to encode logic information in MolFCN cells. (b) The basic structure of a Single Molecule Junction (SMJ). (c) Proposed SMJ-based readout system permitting the detection of driver molecule dipole moment (μ).

form. Indeed, in recent years, SMJs underwent significant improvements, enabling molecular-scale computing and sensing capabilities [18]–[22]. It has been recently demonstrated also the possibility of integrating SMJs with CMOS on the same chip [23]. Fig. 1(b) depicts the structure of an SMJ, composed of a three-oligo(phenylene ethynylene) (OPE3) molecule, between two gold nanoelectrodes (source S and drain D). The molecule is linked to the electrodes through thiol anchoring groups (-SH). A gate electrode couples the molecular channel to an external electric field to modulate the SMJ transport properties [24]. We selected the OPE3 molecular channel for its well-documented theoretical and experimental studies and its recently proven sensing capabilities [25], [26]. Moreover, the gate electrode can be exploited to boost or tune the sensor sensitivity and properties [24]. Fig. 1(c) schematically represents the working principle of the proposed sensor. We assume that the different logic polarization of a MolFCN molecule, i.e., the different molecule dipole moment μ, alters the OPE3 transmission, thus changing its current. Indeed, the ultrasensitive electrical detection of chemical species through SMJ is made possible because of the analyte-sensor electrostatic/chemical interactions. The interactions provoke

conformation or polarization changes in the sensor molecular channel, thus altering the SMJ current [21], [27].

The significant junction current variations based on the driver molecule's dipole orientation demonstrate the feasibility of this approach for dipole discrimination. This confirms that SMJs offer a viable method for distinguishing logic '0' and '1' in a MolFCN circuit. Overall, this work presents a concrete solution for MolFCN readout via SMJs, addressing key scalability, integration, and operability challenges while paving the way for practical MolFCN-CMOS interfacing toward hybrid integration.

II. METHODOLOGY

This work uses SMJs for purely electrostatic sensing of a molecular dipole. Indeed, as shown in Fig. 1(c), the SMJ is subjected to the influence of a single-molecule, here named *driver*, encoding information in the molecular dipole moment (μ). By fixing the SMJ bias voltage (V_{DS}), we expect two different SMJ currents (I_{DS}) depending on the driver μ direction. Fig.2 (a) reports the ideal driver molecule, composed of a saturated chain with an oxygen-based group and an amine group at the two ends. Since our simulation framework does not support oxidized systems, as in real MolFCN systems, we choose a driver with a large permanent dipole of the order of oxidized compounds. To this purpose, we do not consider hydroxy groups but bare oxygen terminations. The driver dipole establishes a local electric field, mimicking the behavior of a MolFCN-compatible molecule. Specifically, we associate the logical state '0' or '1' to the two orientations of the driver, denoted as Dr0 and Dr1, respectively. The two longitudinal orientations define two distinct configurations, supporting the analysis of junction currents for the respective logic states.

The geometries of the driver and the sensor channel OPE3 molecule are optimized through Density Functional Theory (DFT) at the Unrestricted Kohn-Sham level with ORCA, employing the CAM-B3LYP functional and def2-TZVP basis set [28], [29]. Grimme D3 correction is applied for optimization, while D4 enhances accuracy in single-point calculations [30]–[32].

Once optimized, the OPE3 molecule is inserted into a molecular junction formed by Au(111) electrodes with suitable thiol linkers and gold leads, as in Fig.2 (b). The electronic transport properties are analyzed by comparing the current response of the isolated OPE3 junction to that of the system incorporating the driver at three distinct distances d (see Fig.2 (b)): 0.8 nm, 1.2 nm, and 1.6 nm. The system is further examined in each of these configurations with the driver rotated 180° between them, effectively reversing its dipole moment and thus changing the configuration from '0' to '1' (Fig.2 (b)). The currents I_0 and I_1 are hereafter associated to the two logic configurations.

The SMJ transport properties are calculated in QuantumATK v. 2023.12 [33] exploiting the Non-Equilibrium Green's Function (NEGF) formalism. The electronic structure calculations are performed via the Slater-Koster Density Functional Tight Binding (SK-DFTB) method [34], [35].

The transport and electrostatics equations are solved self-consistently, applying periodic boundary conditions along x and Dirichlet conditions in y and z to avoid simulation artifacts due to the presence of the driver. The Poisson equation is solved through the conjugate gradient method. The sampling density in the k-space is set to [4,4,150], with an energy grid cutoff of 10 hartree and a maximum interaction distance of 10 Å. The current I_{DS} for the OPE3 sensor in blank conditions and in the two configurations I_0 and I_1 is determined through the Landauer's equation [36]:

$$I_{DS} = \frac{2q}{h} \int_{-\infty}^{+\infty} T(E, V_{DS}) \left[f_S(E) - f_D(E) \right] dE \quad (1)$$

where q is the elementary charge, h Planck's constant, E the electron energy, and f_S and f_D are the Fermi-Dirac distributions of the S and D, respectively. T is the so-called transmission spectrum. It measures the electron transmission from S to D as a function of E and V_{DS}, and it includes the quantum mechanical nature of the system under analysis. In equation 1, the current is linked to T through an integral that is weighted by the difference in Fermi functions $f_S(E) - f_D(E)$. Thus, the part of T mainly affecting I_{DS} corresponds to E between the S and the D Fermi levels (called Bias Window - BW) [24].

To elucidate the variations in T and I_{DS} across the two logic configurations, we employ the Transmission Pathways (TPs) [37]. They quantify the electron transmission between neighboring atomic sites and are visually depicted by arrows, whose color is the phase shift of the transmission operator.

III. RESULTS

This section presents the proposed readout system. At first, the section introduces the basic schematic used for analyzing the molecular system with DFT calculation by showing the SMJ and the test molecule. Therefore, we demonstrate the effect of the test molecule on the SMJ, thus showing the readout system principle. We test the proposed system on several intermolecular distances and with different bias voltages. Finally, the section introduces the gate effect, demonstrating the properties can be tuned to improve the readout capabilities.

A. OPE3-SMJ as dipole orientation sensor

The calculated driver molecule dipole moment results $\mu(x, y, z) = (1.48926, 0.02522, 15.28786)$ a.u., corresponding to $|\mu| = 39$ D. Fig.2 (c) reports the $I_{DS}(V_{DS})$ curves, for V_{DS} ranging from 0 to 0.5 V, with d=0.8 nm. The red line represents the OPE3 junction current without the driver, whereas the black and blue lines correspond to I_1 and I_0, respectively. The I_{DS} Negative Differential Resistance (NDR) region between 0.35 V and 0.5 V is due to the charging of the OPE3 levels [24]. Indeed, we verify that the applied V_{DS} shifts up the OPE3 levels and T peaks, by reducing their coupling with the S and D electrodes, thus reducing the magnitude of the conducting T peaks within the bias window (BW) (not reported here for brevity). This is a common phenomenon in SMJs [24]. Interestingly, we observe
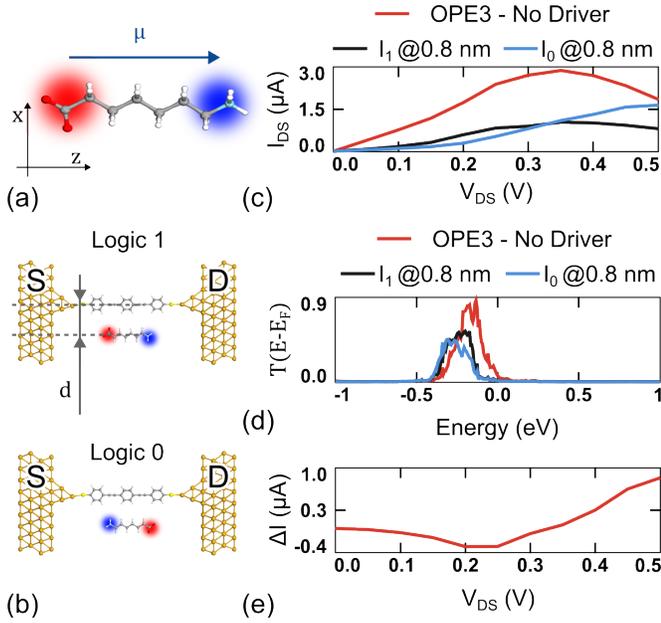
Fig. 2. (a) Ideal molecule used in this work to model the driver molecule. (b) SMJ-driver structure utilized in the simulation, with the driver's orientation encoding the logic states. The driver is positioned at a distance d from the SMJ. (c) IV characteristics for OPE3, I_0, and I_1 when $d = 0.8$ nm. The driver's presence reduces the current in the SMJ for both cases. (d) Transmission spectrum for OPE3, I_0, and I_1 at $d = 0.8$ nm. The transmission probability decreases in the Dr0 and Dr1 cases. (e) Current difference measured as $I_0 - I_1$ for V_{DS} ranging from 0 V to 0.5 V. ΔI reaches a maximum of 0.84 μA at $V_{DS} = 0.5$ V.

a current reduction in both I_1 and I_0 w.r.t. the baseline current of the OPE3. Indeed, the driver presence in both the '0' and '1' configurations modifies the transmission spectrum by shifting down the peaks around the Fermi level (0 V) and reducing their heights - see Fig.2 (d). These effects likely arise due to the electrostatic interaction between the driver and the OPE3 SMJ, leading to a polarization of the OPE3 channel with subsequent energy level shifts and transmissivity modification. Fig.2 (e) shows the key finding for the proposed sensing application. It presents the current difference ΔI between I_0 and I_1. The curve exhibits an increase from 0 V to 0.5 V, reaching a maximum difference of 0.84 μA, with I_0 consistently higher than I_1. These results showcase the potential of the SMJ as a dipole orientation sensor, with ΔI detectable by modern CMOS circuits.

We confirm our hypothesis through a TP analysis, reported in Fig.3. Since the maximum current deviation for both the '0' and '1' configuration is obtained at 0.5 V, we plot the TPs calculated at 0.5 V for the E values corresponding to the maxima of the TS portions included in the BW - arrows in Fig.3(a). The isolated OPE3 TPs are reported in Fig.3(b), while for the OPE3 with the driver in '1' and '0' configurations the TPs are reported in Fig.3(c) and Fig.3(d), respectively. The presence of the driver indeed affects the electron transmission properties by increasing the number of D-to-S electron reflection paths (yellow arrows) in between the phenyl groups - dashed circles in Fig.3. The driver dipole moment polarizes the OPE3 and reduces the amount of
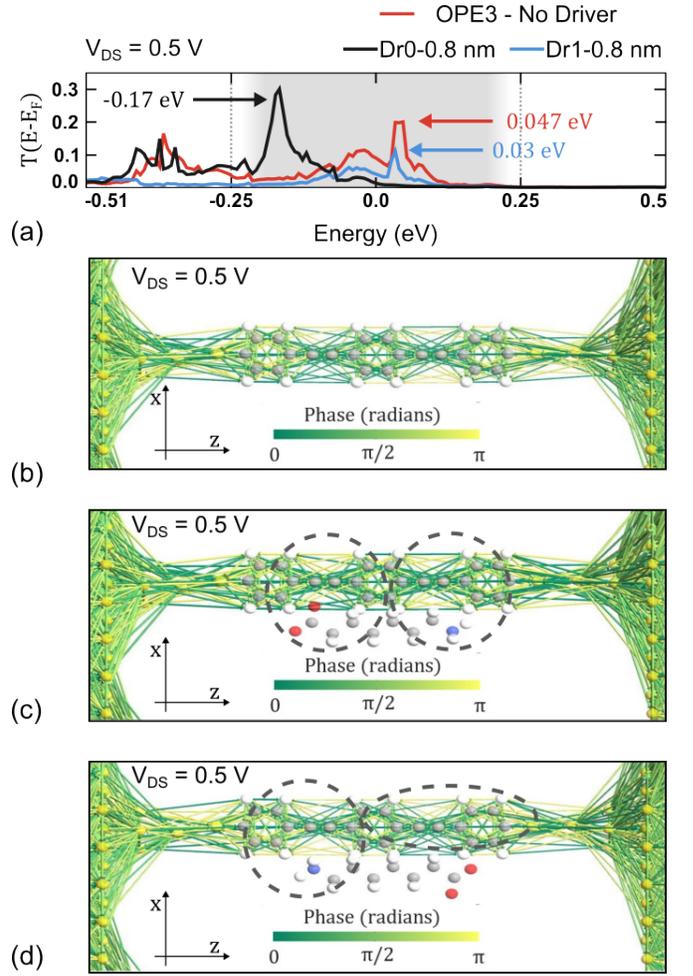

Fig. 3. TPs at 0.5 V of the main T peaks within the BW energy range: -0.17 eV, 0.047 eV and 0.03 eV for OPE3 SMJ, I_0 and I_1, respectively. (a) Transmission spectrum evaluated at $V_{DS} = 0.5$ V for the three considered configurations. (b) OPE3 SMJ; (c) OPE3 SMJ with the driver in '1' configuration; (d) OPE3 SMJ with the driver in '0' configuration.

conjugation at the boundaries of the phenyl groups. Thus, the reflections increase in the OPE3 regions where a minimum amount of electron states are present, i.e., the phenyl ring connectors. As a result, the current is relevantly changed, and at 0.5 V it is almost halved due to the driver presence.

To further analyze the SMJ-based readout, Fig.4 (a) presents I_0 and I_1 for increased distances d=1.2 nm (solid lines) and d=1.6 nm (dashed lines). In both cases, I_0 remains higher than I_1 at the maximum bias of 0.5 V, consistent with the findings at d=0.8 nm. Notably, the maximum current for I_1 increases with distance, reaching 1.07 μA at d=1.2 nm and 1.28 μA at d=1.6 nm, while I_0 remains nearly unchanged at 1.58 μA and 1.59 μA for d=1.2 nm and d=1.6 nm, respectively. Fig.4 (b) presents the ΔI for the three analyzed distances. The largest difference occurs at d=0.8 nm (red curve), maintaining higher values across the V_{DS} range. For d=1.2 nm and d=1.6 nm (black and blue curves), ΔI decreases with distance, indicating a reduced driver influence. Fig.4 (c) further illustrates this trend, showing ΔI at $V_{DS} =$ 0.5 V: 0.84 μA at 0.8 nm, 0.51 μA at 1.2 nm, and 0.32 μA
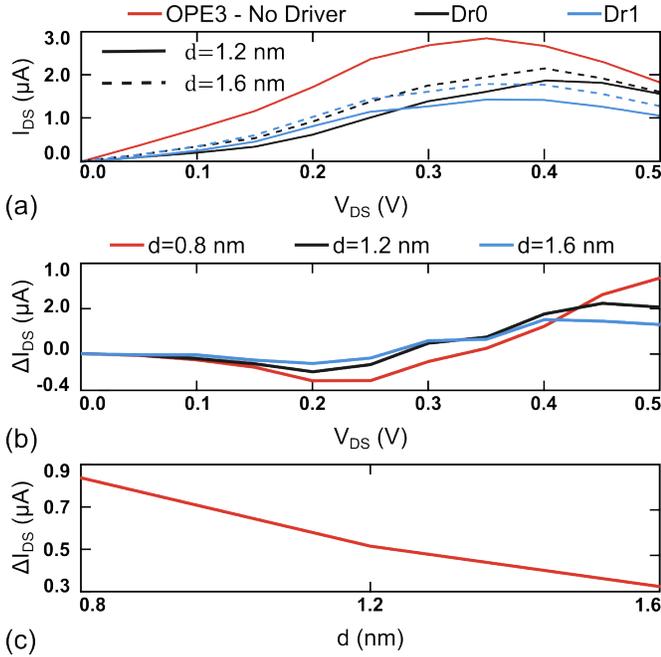
Fig. 4. (a) OPE3 junction current, I_{DS} with and without driver molecule evaluate for different logic, Dr0 and Dr1, and different distances, d. (b) Current difference evaluated for different distances, d. (c) Current difference evaluated for different distance at fixed bias $V_{DS} = 0.5$ V. As the distance increases, the currents I_0 and I_1 approach those in the no-driver case. Consequently, ΔI decreases with the increasing distance.

Fig. 5. IV characteristics in the range of [-0.5, 0.5] V for (a) $d = 8$ nm and (b) $d = 1.2$ nm. ΔI shows an almost symmetric behavior around $V_{DS} = 0$ V, with I_1 being higher than I_0 in absolute terms for negative biases.

at 1.6 nm. This decreasing trend in the current difference between the two driver configurations is accompanied by an increase in the overall current. By increasing the distance between driver and SMJ, the overall current resembles the current of the SMJ without the driver. This result highlights the impact of driver proximity on the transport within the SMJ, pointing out a possible technological challenge in the suitable precise spacing of the SMJ and the MolFCN circuit.

Overall, the results validate the proposed SMJ-based readout as suitable for MolFCN applications. They preliminary show measurable current difference for a distance which is comparable to those used in recently proposed MolFCN devices [11], [12], making the analysed device promising for MolFCN-CMOS integration.

B. Negative V_{DS} analysis

To further investigate the proposed SMJ, we apply negative values V_{DS} to seek the bias point maximizing the current difference between I_0 and I_1 currents. Therefore, we investigate the [-0.5, 0] V range for the d=0.8 nm and d=1.2 nm cases. Fig.5 (a) and Fig.5 (b) show the resulting curves. In both cases, the ΔI presents an almost symmetric behavior with respect to $V_{DS} = 0$ V, with higher values obtained for positive biases. Specifically, ΔI equals 0.62 μA and 0.4 μA at 0.8 nm and 1.2 nm, respectively, when V_{DS}=-0.5 V is applied. Interestingly, both graphs show that, for positive bias values, the I_0 current is higher than I_1, whereas the opposite occurs for negative bias values, as evident at V_{DS}=-0.5 V in Fig.5 (a) and (b). This behavior highlights the impact of the
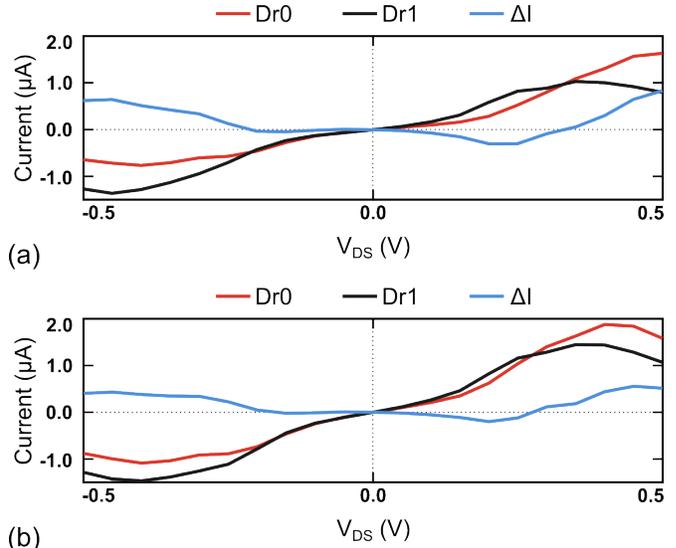
dipole orientation on the SMJ and suggests the possibility of tailoring the sensing mechanism based on the applied bias to optimize the readout of a given logical state. By tuning the bias, the SMJ current can be enhanced in the presence of a dipole oriented accordingly. Furthermore, even with negative currents, a maximum applied voltage $|V_{DS}|$=0.5 V is sufficient to achieve significant current differences.

C. Metallic gate influence on readout performance

Our previous results demonstrate the possibility of tuning the sensing performance of SMJs through an electrostatically coupled gate electrode [24]. The gate enables tuning the SMJ conduction through a suitable T energy shift (toward lower/higher E for positive/negative V_{GS}), that boosts the SMJ sensitivity by including modulated T peaks within the BW. Thus, in the context of MolFCN readout, introducing a gate electrode permits maximizing the current difference ΔI, and the readout capabilities. To evaluate the effect of the gate, we consider the case with d=1.2 nm, and we introduce a 0.6 nm HfO$_2$ (relative permittivity $\epsilon_r = 25$) layer on an ideal metallic gate electrode. Fig. 6(a) shows the employed structure. The chosen HfO$_2$ thickness corresponds to a single atomic layer of dielectric, sufficient for this conceptual study.

We performed the analysis within the voltage range $V_{GS} \in [-3, 3]$ V while keeping constant $V_{DS} = 0.5$ V. This V_{DS} value was found to yield the maximum current difference in the absence of the gate in III-A. Fig. 6(b) and Fig. 6(c) illustrates the variation in the transmission spectrum for different V_{GS} in Dr0 and Dr1 cases, respectively. For increasing V_{GS} values, T shifts towards lower energies, removing transmission peaks from the bias window, and leading to a gradual reduction in current and current difference. Interestingly, negative V_{GS} values push the energy levels within BW, thus increasing I_0, I_1, and, consequently, ΔI, maximizing the sensitivity. Fig. 6(d) confirms the expectations by showing
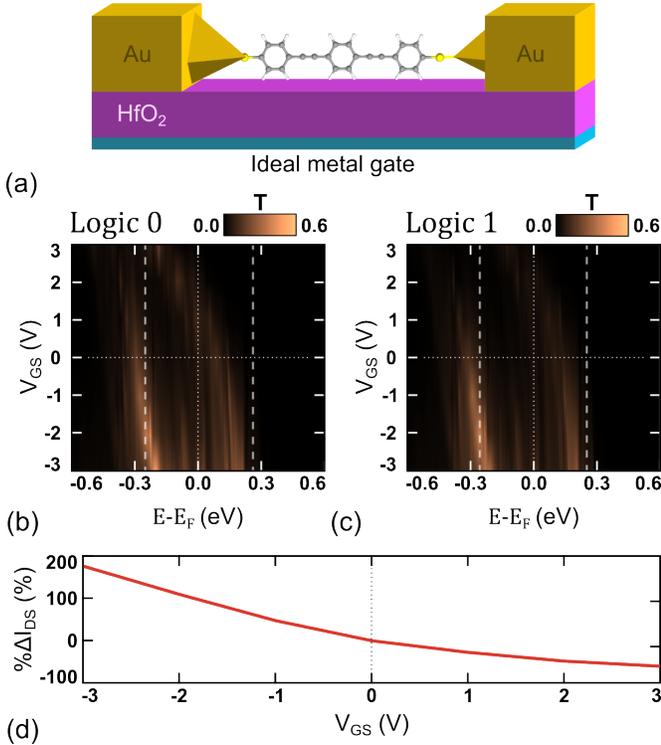
Fig. 6. (a) Representation of the simulated structure, including the device gate electrode, modeled as an ideal metal gate in the simulations. (b)-(c) Transmission spectrum modulation with varying V_{GS} for Dr0 (b) and Dr1 (c) while applying V_{DS}=0.5 V. In both cases, the number of transmission peaks in the BW increases as V_{GS} decreases. (d) Percentage variation of the current difference with respect to V_{GS}. ΔI decreases by 50% at V_{GS}=3 V and increases by nearly 80% at V_{GS}=-2 V.

the percentage variation of I_0, I_1, and ΔI with respect to the reference condition, i.e. $V_{GS} = 0$ V, $V_{DS} = 0.5$ V. The current difference remains nearly unchanged for $V_{GS} = 1$ V and $V_{GS} = 2$ V but is almost halved at V_{GS}=3 V. In contrast, a negative gate-source voltage increases I_0, I_1, and ΔI, with the latter reaching an 80% increase when V_{GS}=-2 V.

In this analysis, the small gate dielectric thickness clearly results in a strong coupling between the gate and the SMJ, significantly impacting current variations. Despite the considered very ideal conditions, the results highlight the crucial role of V_{GS} in enhancing sensing performance. The gate voltage can be used to increase the current difference between the two logic states encoded by the driver dipole orientation. Future work should focus on improving the realism of the gate implementation to further assess and tune its impact on MolFCN readout system.

IV. Conclusion

This work presents a novel approach for MolFCN readout by using Single-Molecule Junctions (SMJs) as amperometric sensors. The proposed method focuses on the electrostatic interaction between a molecule, possibly polarized to encode information in the dipole moment, and an SMJ. In this work, we study the system by modelling the MolFCN molecule with an ideal linear polar molecule. The ideal molecule induces significant and distinguishable current variations which

depends on the encoded logic information, i.e. the dipole moment. The current differences between the two logic states appear detectable by conventional CMOS devices, suggesting that SMJs could provide a viable, scalable, and integrable readout solution while preserving the low-power benefits of MolFCN. However, further simulation and experimental analyses are needed to confirm these findings. Additionally, applying negative V_{DS} and, more importantly, gate voltages can improve sensor sensitivity, allowing for fine-tuning to target specific logic states and maximize the measurable current difference. Future work should focus on refining the simulations presented in this study by introducing variations in the distance and dipole orientation of the molecule interacting with the SMJ. This will help develop a sensor model to integrate into the electronic readout circuit design. From a physical perspective, testing different molecules beyond the OPE3 will be essential to identify alternatives that maximize sensor sensitivity while ensuring integrability and manufacturability.

References

[1] C. S. Lent, B. Isaksen, and M. Lieberman, "Molecular quantum-dot cellular automata," *Journal of the American Chemical Society*, vol. 125, no. 4, pp. 1056–1063, 2003.

[2] Y. Ardesi, M. Graziano, and G. Piccinini, "A model for the evaluation of monostable molecule signal energy in molecular Field-Coupled nanocomputing," *J. Low Power Electron. Appl.*, vol. 12, no. 1, p. 13, Mar. 2022.

[3] V. Arima, M. Iurlo, L. Zoli, S. Kumar, M. Piacenza, F. Della Sala, F. Matino, G. Maruccio, R. Rinaldi, F. Paolucci *et al.*, "Toward quantum-dot cellular automata units: Thiolated-carbazole linked bisferrocenes," *Nanoscale*, vol. 4, no. 3, pp. 813–823, 2012.

[4] G. Beretta, Y. Ardesi, M. Graziano, and G. Piccinini, "Multi-molecule field-coupled nanocomputing for the implementation of a neuron," *IEEE Transactions on Nanotechnology*, vol. 21, p. 52 – 59, 2022.

[5] Y. Wang and M. Lieberman, "Thermodynamic behavior of molecular-scale quantum-dot cellular automata (qca) wires and logic devices," *IEEE Transactions on Nanotechnology*, vol. 3, no. 3, pp. 368–376, 2004.

[6] Y. Ardesi, A. Gaeta, G. Beretta, G. Piccinini, and M. Graziano, "Ab initio molecular dynamics simulations of field-coupled nanocomputing molecules," *Journal of Integrated Circuits and Systems*, vol. 16, no. 1, pp. 1–8, 2021.

[7] R. Listo, F. Ravera, G. Beretta, Y. Ardesi, G. Piccinini, and M. Graziano, "Unveiling charge dynamics in molecular field-coupled nanocomputing," in *2024 IEEE 24th International Conference on Nanotechnology (NANO)*. IEEE, 2024, pp. 424–429.

[8] Y. Ardesi, G. Beretta, F. Mo, C. E. Spano, G. Piccinini, and M. Graziano, "Unveiling field-coupled nanocomputing: Leaning molecules to shape readable bits," *Nano Res.*, vol. 17, no. 9, pp. 8447–8454, Sep. 2024.

[9] F. Ravera, G. Beretta, Y. Ardesi, M. Krzywiecki, M. Graziano, and G. Piccinini, "A roadmap for molecular field-coupled nanocomputing actualization," in *2023 IEEE Nanotechnology Materials and Devices Conference (NMDC)*. IEEE, 2023, pp. 212–213.

[10] R. Listo, F. Mo, F. Ravera, Y. Ardesi, M. Vacca, G. Piccinini, M. Krzywiecki, A. Vezzoli, and M. Graziano, "Unfolding potential and challenges in molecular field-coupled nanocomputing," *Nano Futures*, 2025.

[11] F. Ravera, Y. Ardesi, G. Piccinini, and M. Graziano, "Technology-aware simulation for prototyping molecular field-coupled nanocomputing," *IEEE Transactions on Nanotechnology*, 2024.

[12] Y. Ardesi, U. Garlando, F. Riente, G. Beretta, G. Piccinini, and M. Graziano, "Taming molecular field-coupling for nanocomputing design," *ACM Journal on Emerging Technologies in Computing Systems*, vol. 19, no. 1, pp. 1–24, 2022.

[13] E. Blair, "Electric-field inputs for molecular quantum-dot cellular automata circuits," *IEEE Transactions on Nanotechnology*, vol. 18, pp. 453–460, 2019.

[14] M. I. Rahaman, G. P. Szakmany, A. O. Orlov, and G. L. Snider, "Charge detection towards the readout of bistable charge states in molecular qca," in *2024 IEEE 24th International Conference on Nanotechnology (NANO)*. IEEE, 2024, pp. 277–282.

[15] P. Cong, A. Rocque, and E. P. Blair, "Circuits for the spectroscopic readout of bits from molecular quantum-dot cellular automata," *Journal of Applied Physics*, vol. 136, no. 13, 2024.

[16] N. Liza, D. Murphey, P. Cong, D. W. Beggs, Y. Lu, and E. P. Blair, "Asymmetric, mixed-valence molecules for spectroscopic readout of quantum-dot cellular automata," *Nanotechnology*, vol. 33, no. 11, p. 115201, 2021.

[17] M. I. Rahaman, G. P. Szakmany, A. O. Orlov, and G. L. Snider, "Dipole charge detection: towards the readout of bi-stable charge states in molecular qca," *IEEE Sensors Letters*, 2023.

[18] T. Li, V. K. Bandari, and O. G. Schmidt, "Molecular electronics: Creating and bridging molecular junctions and promoting its commercialization," *Adv. Mater.*, vol. 35, no. 22, p. e2209088, Jun. 2023.

[19] X. Xie, P. Li, Y. Xu, L. Zhou, Y. Yan, L. Xie, C. Jia, and X. Guo, "Single-molecule junction: A reliable platform for monitoring molecular physical and chemical processes," *ACS Nano*, vol. 16, no. 3, pp. 3476–3505, Mar. 2022.

[20] Y. Li, C. Yang, and X. Guo, "Single-molecule electrical detection: A promising route toward the fundamental limits of chemistry and life science," *Acc. Chem. Res.*, vol. 53, no. 1, pp. 159–169, Jan. 2020.

[21] F. Mo, C. E. Spano, Y. Ardesi, G. Piccinini, and M. Graziano, "Beyond-cmos artificial neuron: A simulation- based exploration of the molecular-fet," *IEEE Transactions on Nanotechnology*, vol. 20, pp. 903–911, 2021.

[22] C. E. Spano, Y. Ardesi, G. Piccinini, and M. Graziano, "Enhancing the on/off current ratio in single-molecule fet via destructive quantum interference," *IEEE Transactions on Electron Devices*, vol. 69, no. 10, pp. 5906–5912, 2022.

[23] C. W. Fuller, P. S. Padayatti, H. Abderrahim, L. Adamiak, N. Alagar, N. Ananthapadmanabhan, J. Baek, S. Chinni, C. Choi, K. J. Delaney, R. Dubielzig, J. Frkanec, C. Garcia, C. Gardner, D. Gebhardt, T. Geiser, Z. Gutierrez, D. A. Hall, A. P. Hodges, G. Hou, S. Jain, T. Jones, R. Lobaton, Z. Majzik, A. Marte, P. Mohan, P. Mola, 2nd, P. Mudondo, J. Mullinix, T. Nguyen, F. Ollinger, S. Orr, Y. Ouyang, P. Pan, N. Park, D. Porras, K. Prabhu, C. Reese, T. Ruel, T. Sauerbrey, J. R. Sawyer, P. Sinha, J. Tu, A. G. Venkatesh, S. VijayKumar, L. Zheng, S. Jin, J. M. Tour, G. M. Church, P. W. Mola, and B. Merriman, "Molecular electronics sensors on a scalable semiconductor chip: A platform for single-molecule measurement of binding kinetics and enzyme activity," *Proc. Natl. Acad. Sci. U. S. A.*, vol. 119, no. 5, p. e2112812119, Feb. 2022.

[24] F. Mo, C. E. Spano, Y. Ardesi, M. Ruo Roch, G. Piccinini, and M. Graziano, "Design of pyrrole-based gate-controlled molecular junctions optimized for single-molecule aflatoxin b1 detection," *Sensors*, vol. 23, no. 3, 2023.

[25] C. Jia, M. Famili, M. Carlotti, Y. Liu, P. Wang, I. M. Grace, Z. Feng, Y. Wang, Z. Zhao, M. Ding, X. Xu, C. Wang, S.-J. Lee, Y. Huang, R. C. Chiechi, C. J. Lambert, and X. Duan, "Quantum interference mediated vertical molecular tunneling transistors," *Sci. Adv.*, vol. 4, no. 10, p. eaat8237, Oct. 2018.

[26] P. Yu, L. Chen, Y. Zhang, S. Zhao, Z. Chen, Y. Hu, J. Liu, Y. Yang, J. Shi, Z. Yao, and W. Hong, "Single-molecule tunneling sensors for nitrobenzene explosives," *Anal. Chem.*, vol. 94, no. 35, pp. 12 042–12 050, Sep. 2022.

[27] F. Mo, Y. Ardesi, M. R. Roch, M. Graziano, and G. Piccinini, "Investigation of amperometric sensing mechanism in gold–C_{60}–gold molecular dot," *IEEE Sens. J.*, vol. 22, no. 20, pp. 19 152–19 161, Oct. 2022.

[28] F. Neese, "The orca program system," *Wiley Interdisciplinary Reviews: Computational Molecular Science*, vol. 2, no. 1, pp. 73–78, 2012.

[29] ——, "Software update: the orca program system, version 4.0," *Wiley Interdisciplinary Reviews: Computational Molecular Science*, vol. 8, no. 1, p. e1327, 2018.

[30] F. Weigend and R. Ahlrichs, "Balanced basis sets of split valence, triple zeta valence and quadruple zeta valence quality for h to rn: Design and assessment of accuracy," *Physical Chemistry Chemical Physics*, vol. 7, no. 18, p. 3297, 2005.

[31] S. Grimme, J. Antony, S. Ehrlich, and H. Krieg, "A consistent and accurate ab initio parametrization of density functional dispersion correction (dft-d) for the 94 elements h-pu," *The Journal of Chemical Physics*, vol. 132, no. 15, p. 154104, 2010.

[32] S. Grimme, S. Ehrlich, and L. Goerigk, "Effect of the damping function in dispersion corrected density functional theory," *Journal of Computational Chemistry*, vol. 32, no. 7, pp. 1456–1465, 2011.

[33] S. Smidstrup, T. Markussen, P. Vancraeyveld, J. Wellendorff, J. Schneider, T. Gunst, B. Verstichel, D. Stradi, P. A. Khomyakov, U. G. Vej-Hansen *et al.*, "Quantumatk: An integrated platform of electronic and atomic-scale modelling tools," *J. Phys: Condens. Matter*, vol. 32, p. 015901, 2020.

[34] M. Elstner, D. Porezag, G. Jungnickel, J. Elsner, M. Haugk, T. Frauenheim, S. Suhai, and G. Seifert, "Self-consistent-charge density-functional tight-binding method for simulations of complex materials properties," *Phys. Rev. B*, vol. 58, pp. 7260–7268, Sep 1998. [Online]. Available: https://link.aps.org/doi/10.1103/PhysRevB.58.7260

[35] K. Stokbro, D. E. Petersen, S. Smidstrup, A. Blom, M. Ipsen, and K. Kaasbjerg, "Semiempirical model for nanoscale device simulations," *Phys. Rev. B*, vol. 82, p. 075420, Aug 2010. [Online]. Available: https://link.aps.org/doi/10.1103/PhysRevB.82.075420

[36] S. Datta, *Quantum Transport: Atom to Transistor*. Cambridge University Press, 2005.

[37] G. C. Solomon, C. Herrmann, T. Hansen, V. Mujica, and M. A. Ratner, "Exploring local currents in molecular junctions," *Nat. Chem.*, vol. 2, no. 3, pp. 223–228, Mar. 2010.